sciendo

POLISH MARITIME RESEARCH 1 (117) 2023 Vol. 30; pp. 43-53
10.2478/pomr-2023-0005

STUDY ON THE INFLUENCE OF CHAMFER PERFORATION ON HEAVE AND PITCH OF A SINGLE FLOATING PLATFORM

Wei Wang [1, 2, 3]
Sheming Fan [2]
Yunxiang You [1]
Cheng Zhao * [4]
Liqun Xu [3]
Guibiao Wang [3]
Zhiqiang Lu [3]

[1] School of Naval Architecture Ocean and Civil Engineering, Shanghai Jiaotong University, China
[2] Marine Design and Research Institute of China, China
[3] School of Naval Architecture and Maritime, Zhejiang Ocean University, China
[4] School of Naval Architecture, Ocean and Energy Power Engineering, Wuhan University of Technology, China

* Corresponding author: *S19082400004@zjou.edu.cn (C. Zhao)*

ABSTRACT

The aim of this work is to study the influence of chamfered perforation and chamfering on the heave and pitch motion of a single floating wind power platform with an anti-heave device. Firstly, the hydrodynamic performance of a single floating body with different chamfers, or without perforation, is calculated and analysed. Secondly, the motion of a model without perforation and with 35° chamfered perforation is captured and studied in a towing tank. The results show that when the wave height is large and the period is small, the perforated device has a certain effect. When the wave height and period are small, the pitch suppression effect of chamfered perforation is more obvious than that of non-chamfered perforation. When the period and wave height are large, the heave suppression effect of non-chamfered perforation is better than that of chamfered perforation. In experimental research, the perforated floating body has a certain effect on restraining the heave and pitch of a floating body under most working conditions, and the effect of restraining the pitch is obviously better than that of restraining the heave.

Keywords: single floating wind power platform; different chamfered perforation; numerical simulation; experiment; heave plate

INTRODUCTION

There has been much research on restraining the motion response of a floating platform, both at home and abroad. Ciba [1] presented a platform in which 24 holes were cut and the full and punched heave-plate designs were also tested with regular waves of different periods to obtain amplitude characteristics. Zhiqian et al. [2] found that the suppression effect of heave plates on the motion response in the heave direction was better than that of pitch. Zhou et al. [3] used a numerical calculation method to study the hydrodynamic characteristics of a floating wind turbine spar platform under heave plates, with different air permeability and different numbers of holes under the same air permeability. Song and Odd [4] conducted experimental and numerical studies on perforated rectangular plates at forced harmonic heave motions, horizontally submerged at both a deep and shallow submergence. Samuel et al. [5] predicted the hydrodynamic loads on heave plates by computational fluid dynamics methods. Brecht et al. [6] presented a study on the coupling between a fluid solver and a motion solver to perform fluid–structure interaction simulations of floating bodies. Zhu and Lim [7] performed a forced oscillation experiment to effectively obtain the added mass of a floating body, while

changing various related parameters. Gu et al. [8] simulated the forced heave and surge motion of axisymmetric vertical cylindrical bodies with flat and rounded bases and determined the viscous effects generating drag, as well as influencing added mass and radiation damping. Bezunartea et al. [9] built models of one leg of a platform that was equipped with a heave plate without any reinforcements, to study scale effects on the hydrodynamics of this element. Alexander et al. [10] developed an open-source CFD/6-DOF solver by using OpenFOAM for the high-fidelity simulation of offshore floating wind turbine platforms. Lucas et al. [11] carried out a case-study involving a simplified version of the floater of a semi-submersible FOWT and dealt with cases where the incoming flow was composed of more than one frequency; body motions are a combination of periodic components with very different frequencies. Homayoun et al. [12] dealed with a new concept of near-shore combined renewable energy system which integrates a monopile wind turbine and a floating buoy with heave-type wave energy converter. Ciba presents a method for determining the hydrodynamic coefficients of an object based on the free decay test [13]. Dymarski et al. presented the results of selected works related to the wider subject of the research which concerns design and technology of construction, towing, and settlement on the seabed, or anchoring, of supporting structures for offshore wind farms [14]. Ciba et al. presented a design of a floating platform for offshore wind turbines which is a modification of the Spar design and consists of three variable section columns connected to each other by a ballast tank in the lower part of the platform [15].

The influence of the perforated chamfer on the hydrodynamic performance of the heave plate was studied through physical experiments and numerical simulations [16]. The anti-oscillation device with the purpose of reducing the heave and surge effects of the platform was studied [17]. According to the above-mentioned numerical simulation, a new type of chamfer perforation model is adopted. Based on the numerical simulation, the hydrodynamic performance of the two experimental devices with 35° chamfers holes and without holes under different wave heights and frequencies was experimentally studied, and their heave and pitch response curves were analysed.

BASIC THEORY

The main research work of this paper was the numerical simulation and experimental study of the motion of a floating body in waves, and the solution of the flow field around the floating body based on STAR-CCM+.

NUMERICAL SIMULATION OF HYDRODYNAMIC CHARACTERISTICS

NUMERICAL MODEL DESIGN OF HYDRODYNAMIC CHARACTERISTICS

Taking a 5 MW floating wind turbine as a research object, the numerical simulation and physical experimentation of a single-leg model was carried out. The scale ratio of the test model was set as 1:60 and the numerical simulation model was established according to the actual platform size. The test model is shown in Fig. 1 and the model data are given in Table 1.

Table 1 Data sheet of model

Characteristic parameter	Value
Platform draft (m)	20
Height of the buoy above the waterline (m)	12
Height of the buoy below the waterline (m)	14
Height of the heave plate (m)	6
Diameter of the heave plate (m)	24
Height of the buoy (m)	26
Diameter of the buoy (m)	6
Weight (kg)	3.5×10^6

Numerical simulation of the free motion of a single floating body in first-order waves was carried out. Two-phase flow (air and water) was simulated in a continuum using the 'Volume of Fluid Domain' model. The motion of a single floating body with six degrees of freedom was tracked and measured. There were 25 numerical simulation conditions in total, which adopted combinations of 5 wave periods and 5 wave heights, such as those shown in Table 2.

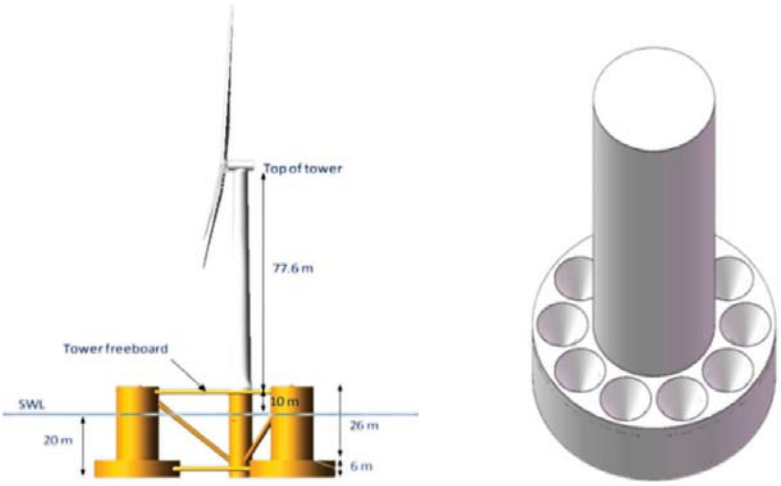

Fig. 1. Schematic diagram of model

Table 2 Numerical simulation conditions

Wave height (m)	Cycle (s)
1.8, 3.6, 5.4, 7.2, 9.0	38.73, 30.98, 25.82, 22.13, 19.36

NUMERICAL COMPUTATION DOMAIN AND BOUNDARY CONDITIONS

A cuboid was used for the calculation domain in the numerical calculations in this paper. The size of the calculation domain was selected as 400 × 240 × 240 m and the corresponding number of meshes was 743,681.

In the setting of boundary conditions, the single floating body was set as a smooth wall; the left side of the calculation domain was set as the velocity inlet, which is the first-order wave velocity. The right side of the calculation domain was set as the pressure outlet, set as hydrostatic pressure. The other surfaces in the calculation domain are symmetrical planes, see Fig. 3.

Mooring settings: the catenary mooring line was adopted with the fairleads at the bottom of the buoy and the bottom of the calculation domain was connected with the catenary. The mass per unit length of the mooring line was 113.4 kg/m and the tensile stiffness was 7.536×10^8 N.

To select the turbulence model, the RANS turbulence model, k-epsilon turbulence, separated flow, constant density, implicitly unsteady, realisable k-epsilon double layer, gradient and other turbulence models were adopted.

The moving grid method was used in the numerical simulation and the translational motion was created in the motion module by the overlapping grid. The motion of a single floating body with six degrees of freedom was tracked and measured.

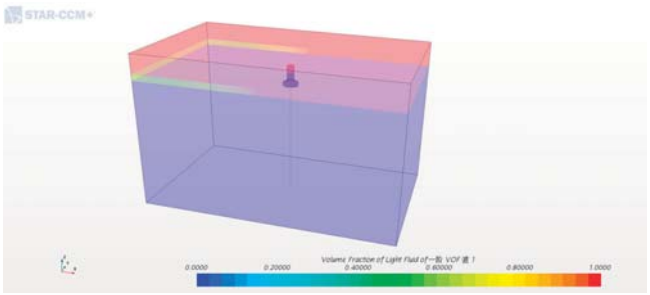

Fig. 3. Schematic diagram of boundary conditions

HYDRODYNAMIC PERFORMANCE AT DIFFERENT WAVE HEIGHTS

The pitch and heave time-domain curves of the maximum perforated model and the non-perforated model under the minimum cycle condition under different wave heights were selected for comparison, as shown in Fig. 4. The symbol 'origin' in the picture means the model without perforation, and the symbol '35°' means the perforation with 35° chamfers.

The movement trend of the perforated model and the model without perforation basically remains the same on the time history curve; the perforation has no obvious anti-rolling effect except the working condition with large wave heights.

Similar to the case of pitch, when the wave height is small, the perforation has no significant effect on the anti-surging of the model but, when the wave height is large, the perforated anti-surge device has a certain anti-surge effect.

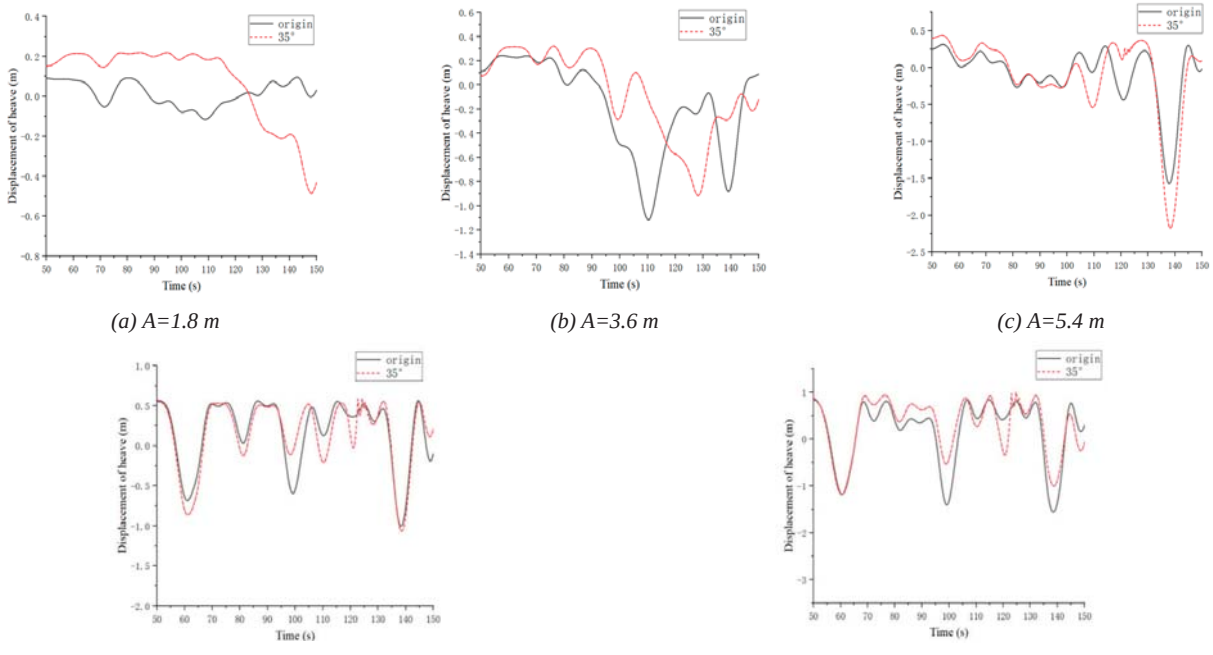

(a) A=1.8 m *(b) A=3.6 m* *(c) A=5.4 m*

(d) A=7.2 m *(e) A=9.0 m*

Fig. 4. Period T = 19.36 s, heave comparison between origin and 35° at different wave heights

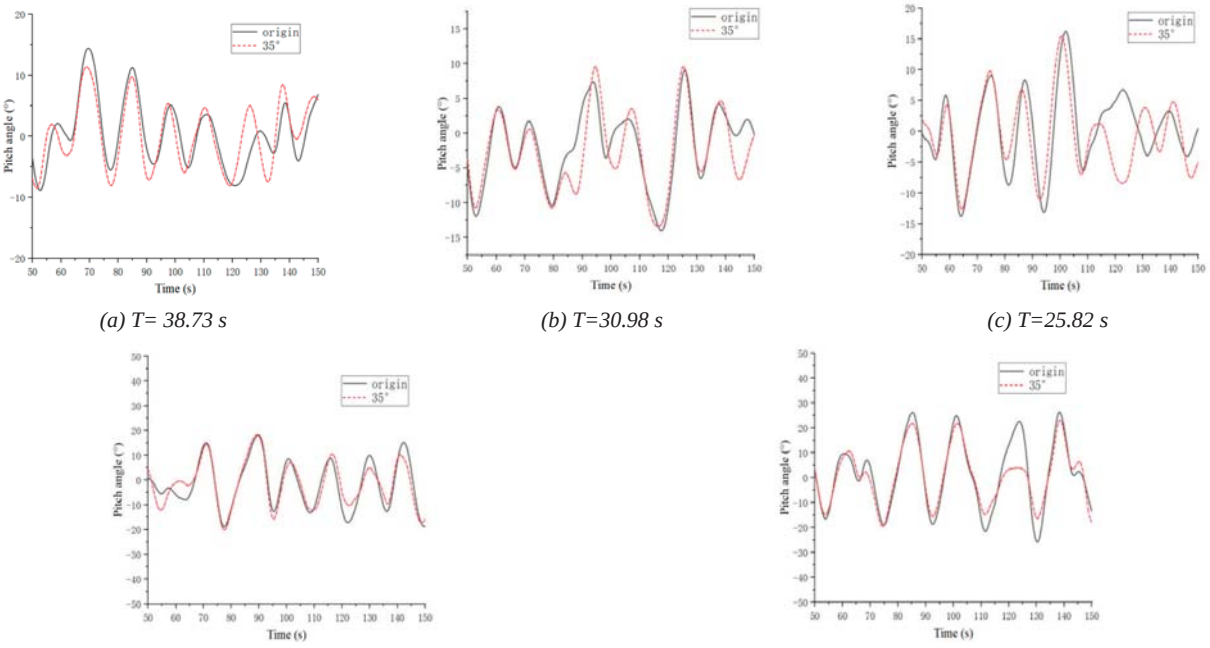

(a) T= 38.73 s *(b) T=30.98 s* *(c) T=25.82 s*

(d) T=22.13 s *(e) T=19.36 s*

Fig. 5. Wave height A = 9 m, pitch comparison of origin and 35° in different periods

HYDRODYNAMIC PERFORMANCE WITH DIFFERENT FREQUENCIES

The pitch and heave time domain curves of the maximum perforated model and the model without perforation under different periods at the maximum wave height condition were selected for comparison, as shown in Fig. 5 and Fig. 6.

On the time history curve of pitching, it can be seen that the perforation only has a certain anti-pitching effect for short periods.

Similar to the case of pitch, the perforating only has a certain effect for short periods but has no obvious effect on the condition of large cycles.

HYDRODYNAMIC PERFORMANCE WITH DIFFERENT CHAMFERS

The multiple maximum pitch angles and maximum heave distances were extracted and the average value taken, to obtain the point line diagram for comparison.

At the same frequency, but with an increase in wave height, the pitch amplitude of different perforated models shows a

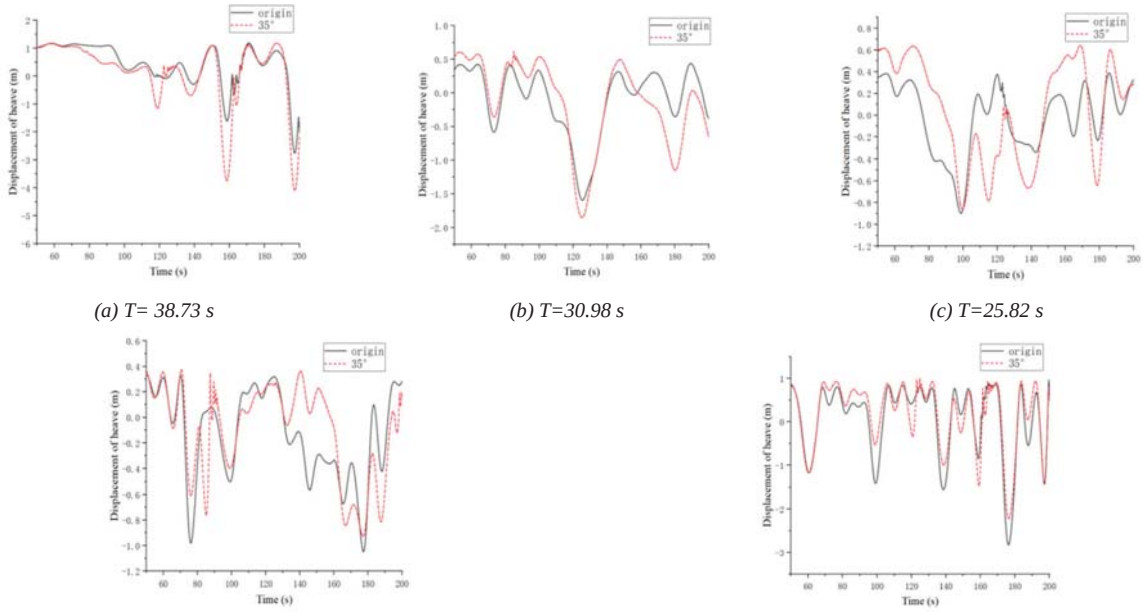

(a) T= 38.73 s *(b) T=30.98 s* *(c) T=25.82 s*

(d) T=22.13 s *(e) T=19.36 s*

Fig. 6. Wave height A = 9 m, heave comparison of origin and 35° in different periods

generally upward trend; the perforated model, basically, has a certain inhibitory effect when the wave height is large. When the wave height is small, the pitch suppression with chamfered perforation is more obvious than that without chamfering but there is no significant difference between them when the wave height is large, as shown in Fig. 7.

In terms of heave, with an increase in wave height, the overall heave amplitude of the platform increases but the anti-heave device with perforations has no significant inhibitory effect on the heave of the platform, which is shown in Fig. 8.

Fig. 9 shows the comparison of pitch at different hole angles and different frequencies but at the same wave height. At the same wave height, the pitch amplitude decreases with the increase in wave period. When the wave height and the frequency are large, the perforation has a certain inhibitory effect on the pitch of the platform. When the wave height and period are small, the pitch suppression effect of the perforation with chamfers is more obvious than that of the perforation without chamfers, but there is no obvious law in other working conditions.

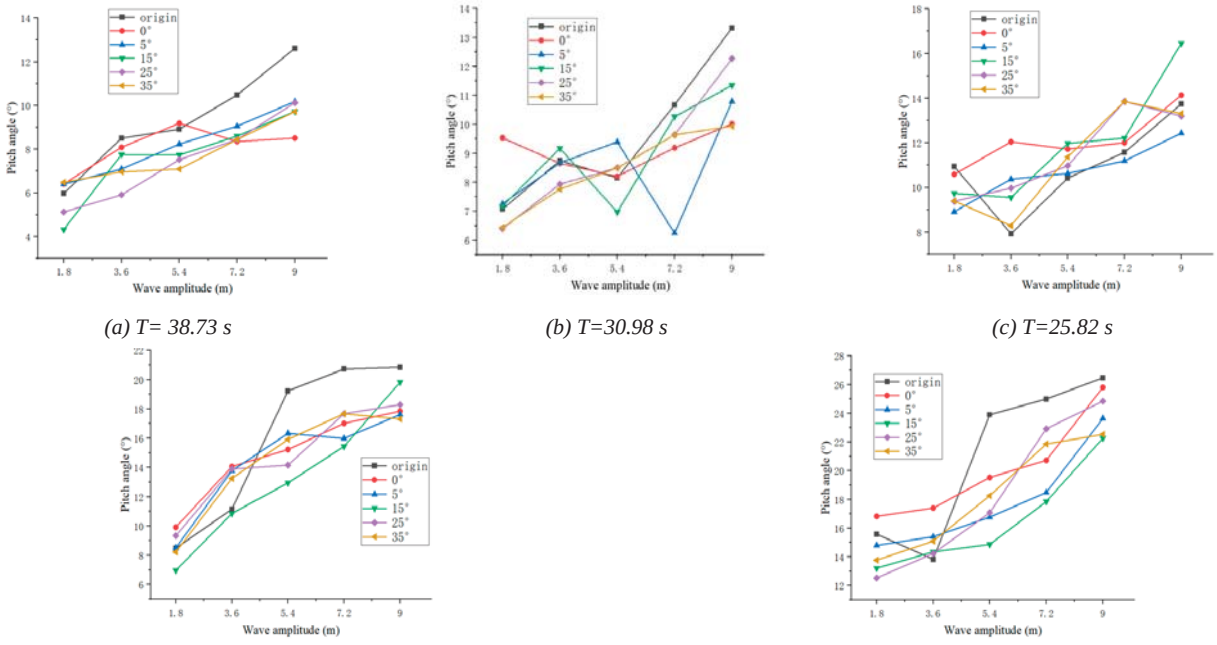

(a) T= 38.73 s *(b) T=30.98 s* *(c) T=25.82 s*

(d) T=22.13 s *(e) T=19.36 s*

Fig. 7. Comparison of pitch with different hole angle in different wave height at the same frequency

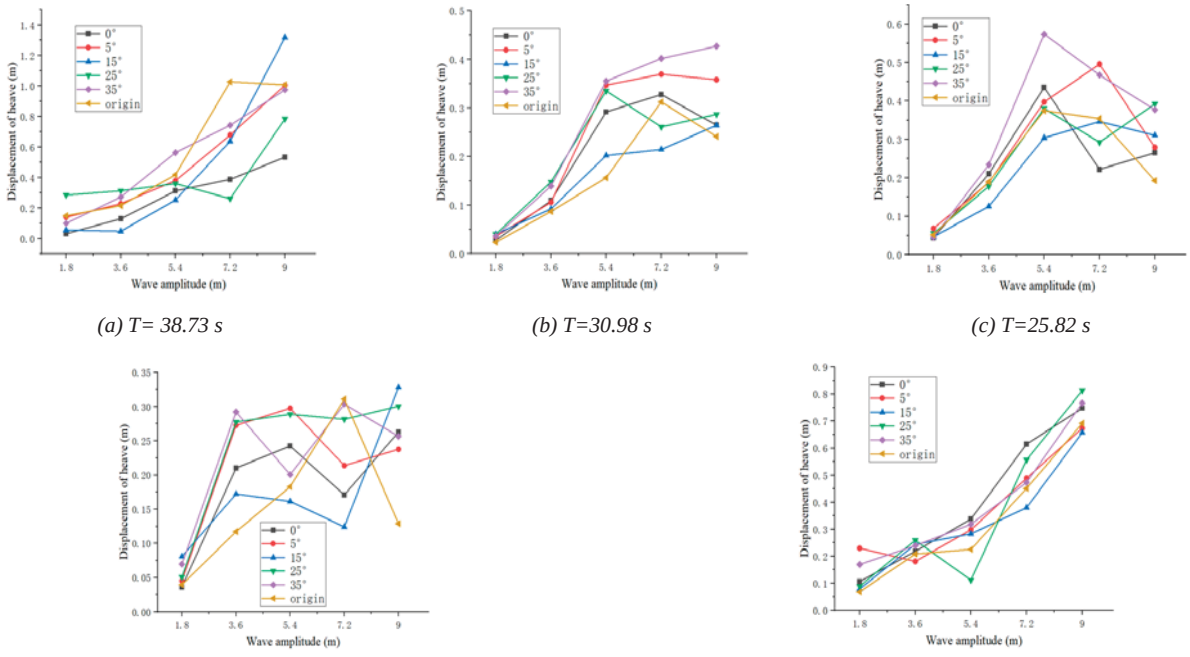

(a) T= 38.73 s *(b) T=30.98 s* *(c) T=25.82 s*

(d) T=22.13 s *(e) T=19.36 s*

Fig. 8. Comparison of heave with different hole angle in different wave height at the same frequency

Fig. 10 shows the comparison of heave with different hole angles in different frequencies at the same wave height. In terms of heave amplitude, the effect of perforation on heave suppression is not obvious under most working conditions. When the period is large, the suppression effect of non-chamfered perforation on heave motion is better than that with chamfered perforation but, when the period is short, the suppression effect of chamfers on heave motion has no obvious law.

EXPERIMENTAL STUDY ON HYDRODYNAMIC CHARACTERISTICS

EXPERIMENTAL DESIGN OF HYDRODYNAMIC CHARACTERISTICS

The experiments were carried out in a towing tank. The pool size was 130 × 6 × 4 m. The wave making system was located at one end of the pool and the corresponding wave

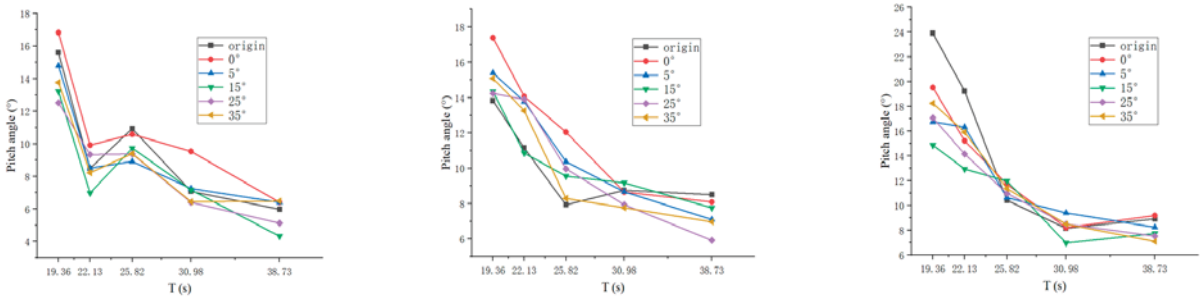

(a) A=1.8 m (b) A=3.6 m (c) A=5.4 m

(d) A=7.2 m (e) A=9.0 m

Fig. 9. Comparison of pitch with different hole angle in different frequencies at the same wave height

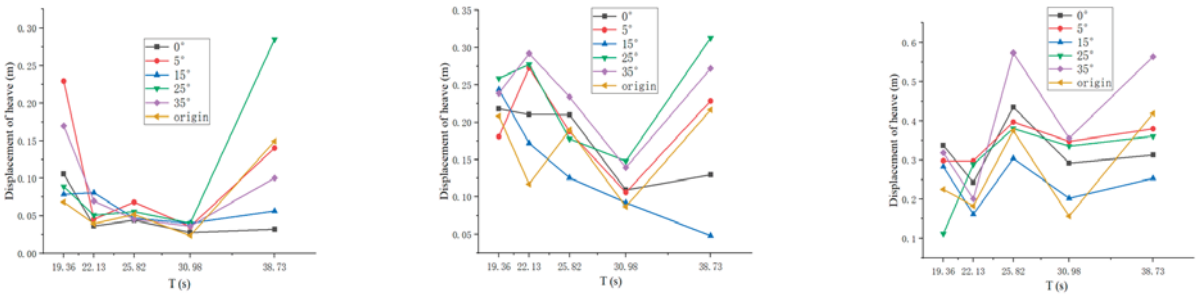

(a) A=1.8 m (b) A=3.6 m (c) A=5.4 m

(d) A=7.2 m (e) A=9.0 m

Fig. 10. Comparison of heave with different hole angle in different frequencies at the same wave height

dissipation system was installed at the other end of the pool.

The motion amplitudes of the single floating body model without perforation and with 35° chamfered perforation, moored in the pool under different working conditions, were measured by the PTI (Phoenix technologies Inc) 3D motion capture system. The sensor used for the company PTI test was installed on the floating body, see Fig. 11 and Fig. 12.

The frequencies were 0.20 s, 0.25 s and 0.30 s, while the wave heights were 0.030 m, 0.066 m and 0.300 m. There were nine working conditions in total, which adopted the combination of three frequencies and three wave heights.

Fig. 11. Installation diagram of single floating body and capture system

Fig. 12. PTI 3D motion capture sensor

SOLUTION OF PLATFORM MOTION

The coordinate relationship between the model reference point (i.e. the centroid G) and any relative fixed point R of the model was as follows:

$$\begin{cases} x = x_G + c_{\xi x}\xi + c_{\eta x}\eta + c_{\zeta x}\zeta \\ y = y_G + c_{\xi y}\xi + c_{\eta y}\eta + c_{\zeta y}\zeta \\ z = z_G + c_{\xi z}\xi + c_{\eta z}\eta + c_{\zeta z}\zeta \end{cases} \quad (1)$$

where (x_G,y_G,z_G) are the spatial motion coordinates of point G; (x,y,z) are the spatial motion coordinates of point R; and (ξ,η,ζ) is the relative coordinate of point R on the model's body coordinate system.

It can be seen that the movement of a certain point on the model can be calculated through the model data and the movement of the centre of gravity of the model. This means that the conversion formula can deduce the movement of the centre of gravity of the model, under the condition that the movement of a certain point on the model is known. Therefore, through the above coordinate conversion method, this paper obtained the actual motion at the centre of gravity of the floating body, which makes the research in this paper more scientific and intuitive.

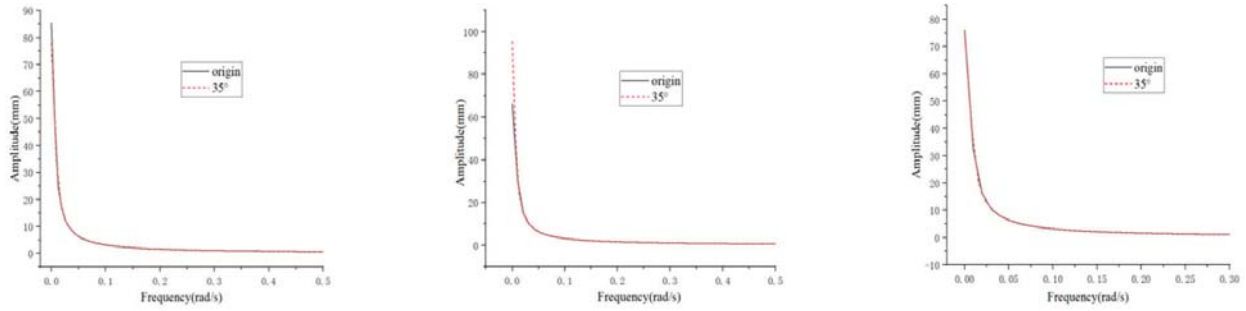

(a) A=0.03 m *(b) A=0.06 m* *(c) A=0.09 m*

Fig. 13. Heave amplitude frequency response curves of models with different wave heights at 0.2 Hz

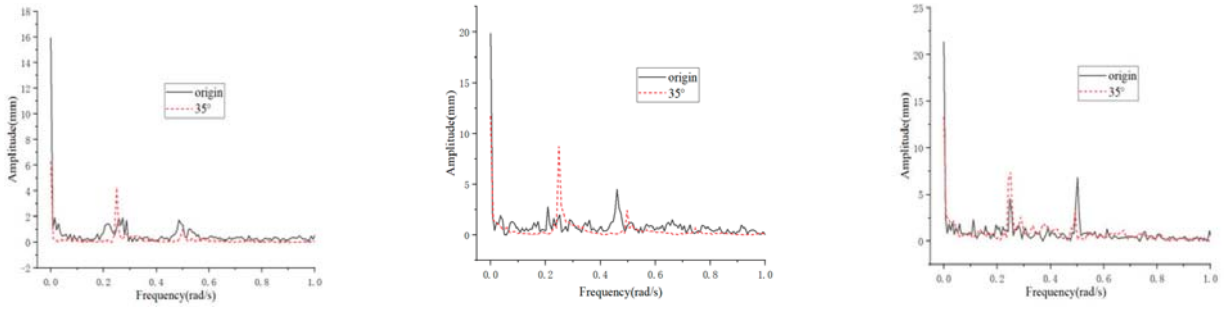

(a) A=0.03 m *(b) A=0.06 m* *(c) A=0.09 m*

Fig. 14. Heave amplitude frequency response curves of models with different wave heights at 0.25 Hz

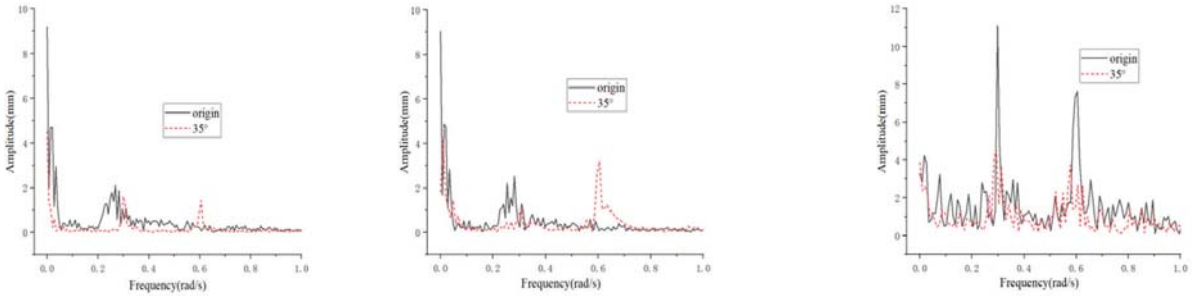

(a) A=0.03 m *(b) A=0.06 m* *(c) A=0.09 m*

Fig. 15. Heave amplitude frequency response curves of models with different wave heights at 0.30 Hz

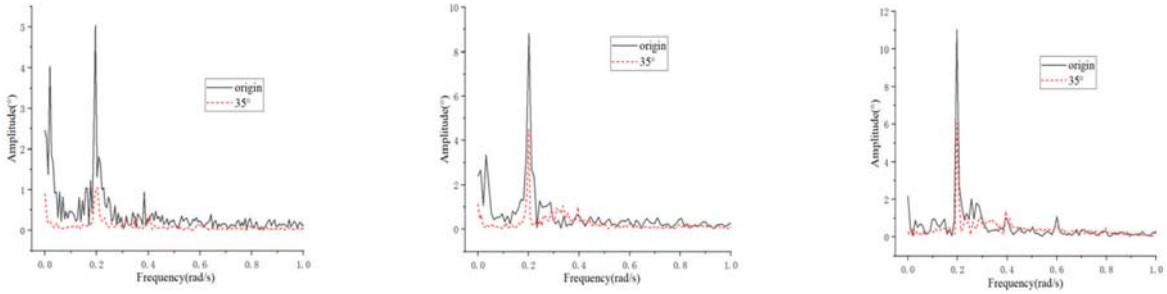

(a) A=0.03 m *(b) A=0.06 m* *(c) A=0.09 m*

Fig. 16. Pitch amplitude frequency response curve at different wave heights at 0.20 Hz

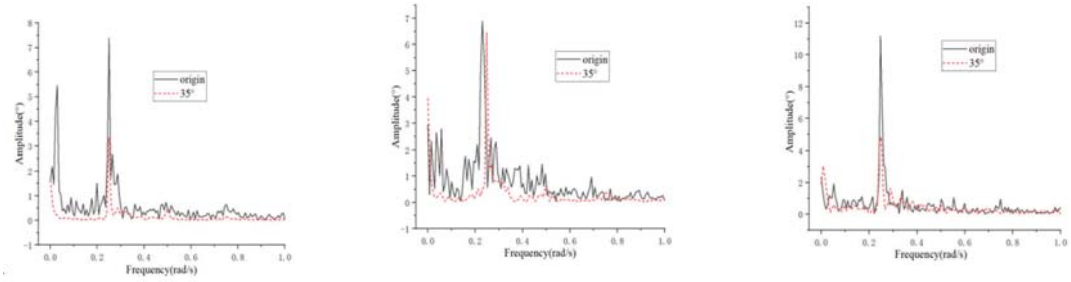

(a) A=0.03 m *(b) A=0.06 m* *(c) A=0.09 m*

Fig. 17. Pitch amplitude frequency response curve at different wave heights at 0.25 Hz

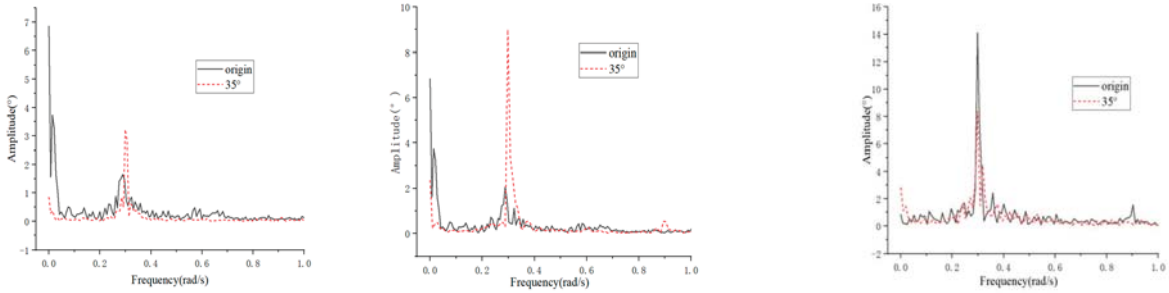

(a) A=0.03 m *(b) A=0.06 m* *(c) A=0.09 m*

Fig. 18. Pitch amplitude frequency response curve at different wave heights at 0.30 Hz

INFLUENCE OF PERFORATION ON HYDRODYNAMIC PERFORMANCE

The motion response of a floating body in heave and pitch, measured by the PTI 3D motion capture system, was drawn to the frequency domain curve by the Fourier transform, and the anti-heave effect of the perforation on the floating body was analysed.

As shown in Fig. 13-15, when the wave frequency is 0.25 Hz and 0.30 Hz, the heave response curve reaches a maximum at the corresponding frequency, and tends to be obvious with the increase of wave height. In addition, there are further maximum values at 0.50 Hz and 0.60 Hz but it is not obvious when the wave frequency is 0.20 Hz.

On the pitch amplitude frequency characteristic curve, the frequency of extreme points in the frequency domain diagram of each working condition corresponded with the experimental wave frequency and, except for a few working conditions, the amplitude of the perforated model is significantly smaller than that of the model without perforation, as shown in Fig. 16, Fig. 17 and Fig. 18.

In order to better compare the suppression effect of perforation on the heave and pitch of a floating body, the standard deviation of heave and pitch amplitudes of the model with 35° perforation and the model without perforation were solved and compared, as shown in the figures below.

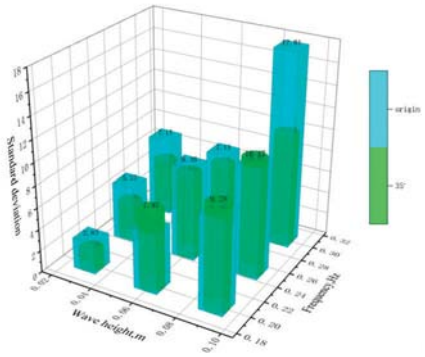

Fig. 19. Comparison of standard deviation of heave at different conditions

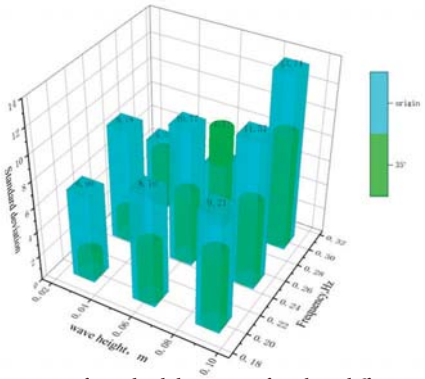

Fig. 20. Comparison of standard deviation of pitch at different conditions

Fig. 19 and Fig. 20 show that the perforations have a positive significance in suppressing the heave and pitch of a floating body.

In terms of suppressing heave, the effect of perforation to reduce heave tends to be obvious, as the wave frequency increases under the same wave height. At the same frequency, the effect of perforation is not obvious when the frequency is small.

With respect to restraining the pitching, the larger the frequency, the anti-pitch effect of perforation showed a generally downward trend. At the same frequency, the higher the wave height, the anti-pitch effect of perforation is more obvious.

COMPARATIVE ANALYSIS OF NUMERICAL SIMULATION AND EXPERIMENTAL RESEARCH

The condition of a wave height at 0.09 m, with frequencies of 0.2 Hz and 0.3 Hz, were taken as examples (LC1, LC2) and the numerical simulation and test results of the movement of the perforated model were analysed for one cycle and compared (see Fig. 21 and Fig. 22).

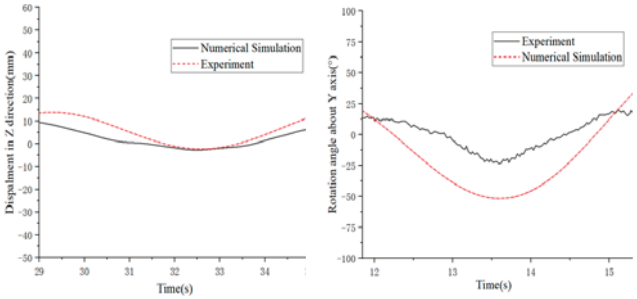

(a)heave *(b)pitch*

Fig. 21. Comparison between numerical simulation and experimental results with 35°at LC1

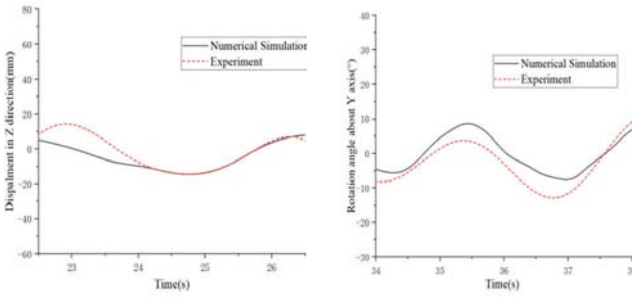

(a)heave *(b)pitch*

Fig. 22. Comparison between numerical simulation and experimental results with 35°at LC2

Although the variation in trends for heave and pitch are basically the same in the cycle, there are still large errors. There may be many reasons for this, such as the different constraints and catenary materials between the simulation and experimental testing of a floating body, and errors in the motion capture of experimental equipment.

CONCLUSIONS

With respect to the numerical simulation, the movement of various models with different chamfers or without perforation are calculated and the effects of chamfered perforation on the heave reduction of a floating body are compared. In the experiment, the motion of models with 35° chamfered perforation or without perforation are compared, and the damping effect of perforation on a single floating wind power platform under different working conditions is analysed.

(1) According to the comparison of motion between the model with 35° chamfered perforation or without perforation in numerical simulation, it can be seen that: when the wave height is small, there is no significant difference between the motion of the two models but, when the wave height is large and the period is small, the perforated device has a certain anti-surge effect.

(2) When the wave height and period are small, the pitch suppression effect of chamfered perforation is more obvious than that of non-chamfered perforation while, in other working conditions, the pitch suppression effect of chamfers of perforation has no obvious law. Meanwhile, when the period and wave height are large, the heave suppression effect of non-chamfered perforation is better than that of chamfered perforation, but there is no obvious law when the period or wave height is small.

(3) With respect to experimental research, the perforation of the floating body has a certain effect on restraining the heave and pitch of the floating body under most working conditions, and the effect of restraining the pitch is obviously better than that of restraining the heave. With an increase in frequency, the suppression effect of perforation on the heave response of the floating body as a whole is enhanced, but the suppression effect on its pitch is gradually weakened.

(4) The numerical simulation and experimental comparison show that the variation trends of heave and pitch are basically the same for one cycle, but there are still large errors. This may be caused by the different constraints and catenary materials between the simulation and the experiments, and errors in motion capture in the experimental equipment.

ACKNOWLEDGEMENTS

This study was financially supported by the General Project of the National Nature Science Foundation of China (grant no. 51679217) and the major research and development project of Daishan County Zhejiang Province (grant no. 202202).

REFERENCES

1. E. Ciba, P. Dymarski and M. Grygorowicz, "Heave Plates with Holes for Floating Offshore Wind Turbines", Polish Marit. Res., vol. 29, no. 1, 2022. doi: 10.2478/pomr-2022-0003.

2. H. Zhiqian, D. Qinwei, and L. Chun, "Research on Heave Motion Inhibition for the Semi-submersible Platform of Floating Wind Turbines with New Heave Plates", Journal of Power Engineering, vol. 39, no. 5, 2019, pp. 402-408.

3. Z. Ye, J. Zhang, G. Zhou, C. Li, "Research on hydrodynamic characteristics of the floating wind turbine with heave plate", Acta Energiae Solaris Sinica, vol. 40, no. 1, 2019. doi: 10.19912/j.0254-0096.2019.01.033. doi: 10.19912/j.0254-0096.2019.01.033.

4. S. An and O. Faltinsen, "An experimental and numerical study of heave added mass and damping of horizontally submerged and perforated rectangular plates", Journal of Fluids and Structures, vol. 39, 2013, pp.87-101. doi: 10.1016/j.jfluidstructs.2013.03.004.

5. S. Holmes, S. Bhat, P. Beynet, A. Sablok, and I. Prislin, "Heave Plate Design with Computational Fluid Dynamics", JOMAE, vol. 123, no. 1,2001. doi: 10.1115/1.1337096.

6. B. Devolder, P. Troch, P. Rauwoens, "Accelerated numerical simulations of a heaving floating body by coupling a motion solver with a two-phase fluid solver", Computers and Mathematics with Applications, vol. 77, 2019, pp.1605-1625. doi: 10.1016/j.camwa.2018.08.064.

7. L. Zhu, H-C. Lim, "Hydrodynamic characteristics of a separated heave plate mounted at a vertical circular cylinder", Ocean Engineering, vol. 131, 2017, pp.213-223. doi: 10.1016/j.oceaneng.2017.01.007

8. H. Gu, P. Stansby, T. Stallard, E. Carpintero Moreno, "Drag, added mass and radiation damping of oscillating vertical cylindrical bodies in heave and surge in still water", Journal of Fluids and Structures, 82, 2018, pp.343-356. doi: 10.1016/j.jfluidstructs.2018.06.012

9. A. Bezunartea-Barrio, S. Fernandez-Ruano, A. Maron-Loureiro, E. Molinelli-Fernandez, F. Moreno-Buron, J. Oria-Escudero, J. Rios-Tubio, C. Soriano-Gomez, A. Valea-Peces, C. Lopez-Pavon, A. Souto-Iglesias, "Scale effects on heave plates for semi-submersible floating offshore wind turbines: case study with a solid plain plate", Journal of Offshore Mechanics and Arctic Engineering, vol. 142, no. 3, 2020. doi:10.1115/1.4045374

10. A.J. Dunbar, B.A. Craven, E.G. Paterson, "Development and validation of a tightly coupled CFD/6-DOF solver for simulating floating offshore wind turbine platforms", Ocean Engineering, vol. 110, 2015, pp.98-105. doi: 10.1016/j.oceaneng.2015.08.066

11. L.H.S.d Carmo, P.C.d Mello, E.B. Malta, G.R. Franzini, A.N. Simos, R.T. Gonc¸ H. Suzuki, "Analysis of a FOWT Model in Bichromatic Waves: An Investigation on the Effect of Combined Wave-Frequency and Slow Motions on the Calibration of Drag and Inertial Force Coefficients", ASME 2020 39th International Conference on Ocean, Offshore and Arctic Engineering. doi: 10.1115/OMAE2020-18239

12. E. Homayoun, H. Ghassemi, H. Ghafari, "Power Performance of the Combined Monopile Wind Turbine and Floating Buoy with Heave-Type Wave Energy Converter", Polish Maritime Research, vol. 26, no. 3, 2019, pp. 107-114. doi:10.2478/pomr-2019-0051.

13. E. Ciba, "Heave Motion of a vertical Cylinder with Heave Plates", Polish Maritime Research, vol. 28, no. 1, 2021, pp. 42-47. doi: 10.2478/pomr-2021-0004.

14. P. Dymarski, C. Dymarski, E. Ciba, "Stability Analysis of the Floating Offshore Wind Turbine Support Structure of Cell Spar Type During Its Installation", Polish Maritime Research, vol. 24, no. 4, 2021, pp. 109-116. doi: 10.2478/pomr-2019-0072.

15. E. Ciba, P. Dymarski, M. Grygorowicz, "Analysis of The Hydrodynamic Properties of the 3-Column Spar Platform for Offshore Wind Turbines", Polish Maritime Research, vol. 29, no. 2, 2022, pp. 35-42. doi: 10.2478/pomr-2022-0015.

16. W. Wang, C. Zhao, P. Jia, Z. Lu, and Y. Xie, "Numerical simulation and experimental study on perforated heave plate of a DeepCwind floating wind turbine platform", Ships and Offshore Structures, vol. 18, no. 3, 2022, pp. 438-449. doi: 10.1080/17445302.2022.2062157.

17. W. Wang, S. Fan, Y. You, C. Zhao, L. Xu, G. Wang. "Numerical and Experimental Study on an Anti-Oscillation Device for the DeepCwind Floating Semi-Submersible Turbine Platform"& Energies, vol. 16, no. 3, 2023, 1034. doi: 10.3390/en16031034